Published in final edited form as:
Langmuir. 2009 October 20; 25(20): 12136–12143. doi:10.1021/la901647n.

A $^{13}C\{^{31}P\}$ REDOR NMR Investigation of the Role of Glutamic Acid Residues in Statherin-Hydroxyapatite Recognition

Moise Ndao[1], **Jason T. Ash**[1], **Nicholas F. Breen**[1], **Gil Goobes**[3], **Patrick S. Stayton**[2], and **Gary P. Drobny**[*,1]

[1]Department of Chemistry, University of Washington, Seattle, Washington 98195

[2]Department of Bioengineering, University of Washington, Seattle, Washington 98195

[3]Department of Chemistry, Bar Ilan University, Ramat Gan 52900, Israel

Abstract

The side chain carboxyl groups of acidic proteins found in the extra-cellular matrix (ECM) of mineralized tissues play a key role in promoting or inhibiting the growth of minerals such as hydroxyapatite (HAP), the principal mineral component of bone and teeth. Among the acidic proteins found in the saliva is statherin, a 43-residue tyrosine-rich peptide that is a potent lubricant in the salivary pellicle and an inhibitor of both HAP crystal nucleation and growth. Three acidic amino acids – D1, E4, and E5 – are located in the N-terminal 15 amino acid segment, with a fourth amino acid, E26, located outside the N-terminus. We have utilized $^{13}C\{^{31}P\}$ REDOR NMR to analyze the role played by acidic amino acids in the binding mechanism of statherin to the HAP surface by measuring the distance between the δ-carboxyl ^{13}C spins of the three glutamic acid side chains of statherin (residues E4, E5, E26) and ^{31}P spins of the phosphate groups at the HAP surface. $^{13}C\{^{31}P\}$ REDOR studies of glutamic-5-^{13}C acid incorporated at positions E4 and E26 indicate a ^{13}C–^{31}P distance of more than 6.5 Å between the side chain carboxyl ^{13}C spin of E4 and the closest ^{31}P in the HAP surface. In contrast, the carboxyl ^{13}C spin at E5 has a much shorter ^{13}C–^{31}P internuclear distance of 4.25±0.09 Å, indicating that the carboxyl group of this side chain interacts directly with the surface. ^{13}C $T_{1\rho}$ and slow-spinning MAS studies indicate that the motions of the side chains of E4 and E5 are more restricted than that of E26. Together, these results provide further insight into the molecular interactions of statherin with HAP surfaces.

Introduction

The remarkable material properties of bone and teeth arise because of the sophisticated crystal engineering capabilities that have evolved in the biological world. Proteins function at the interface between cells and the inorganic phase in these composite hard tissues. The activities of these proteins at the organic-inorganic interface are thus critical not only to the construction of biocomposites with improved mechanical properties but to the maintenance of hard tissue integrity as well. The disruption of these functions has adverse medical and dental ramifications, leading to bone and tooth deterioration, dental calculus formation, atherosclerotic plaque formation, artificial heart valve calcification, kidney and gall stone build-up[1–3].

There has been considerable attention focused on the role of acidic proteins in biomineralization processes[4–10]. It is widely recognized, however, that the molecular details of protein function at the organic-inorganic interface are just beginning to be uncovered. The

[*]Corresponding author. drobny@chem.washington.edu.

significance of pushing this frontier will be found in the development of calcification inhibitors and promoters that could impact orthopedics, urology, dentistry, and cardio-vascular fields. A better understanding of how these proteins recognize and assemble in bioactive fashion on inorganic mineral phases could also aid in the development of surface coatings to improve the biocompatibility of implantable biomaterials and tissue engineering scaffolds.

The mineralization of bone occurs by the deposition of hydroxyapatite (HAP, $Ca_{10}(PO_4)_6(OH)_2$) in the extra-cellular matrix. It has long been hypothesized that acidic protein components of the ECM are involved in the initiation and regulation of mineralization. Bone sialoprotein and osteopontin, for example, are extensively phosphorylated and contain regions that are rich in acidic amino acids[11,12]. Sialoprotein contains two regions consisting of contiguous glutamic acid residues and a RGD cell attachment sequence. The direct involvement of these acidic amino acid regions in HAP nucleation is further supported by studies of the effect of monomeric acidic amino acids and their polymers in HAP nucleation[13]. Both glutamic acid and aspartic acid markedly inhibit the rate of HAP crystal growth[14]. Polyglutamic acid nucleates apatites[15], and polyaspartate increases the amount of calcium phosphate crystals within assembling collagen fibers[16–18].

Acidic ECM proteins play a similarly important role in the regulation of HAP nucleation in the oral cavity. Dentin Matrix Protein 1 is essential in the maturation of odontoblasts and osteoblasts and subsequent dentin mineralization[19]; amelogenin is crucial to proper formation of enamel[20], yet the operations of neither are well understood. Functional studies using NMR measurements carried out on a derivative of amelogenin have shown its structure is largely random coil when adsorbed to hydroxyapatite, and identified 3 residues that are within 7 Å from the surface of HAP[21].

Statherin is an acidic human salivary protein of 43 amino acid residues, DpSpSEEKFLRRIGRFGYGYGPYQPVPEQPLYPQPYQPQYQQYTF (pS=phosphoserine), with a molecular weight of 5.38 kDa. It inhibits both the nucleation and growth of HAP. Previous studies of statherin fragments by Nancollas and coworkers[22,23] showed that the N-terminal 15 amino acid fragment (SN-15, DpSpSEEKFLRRIGRFG, pS=phosphoserine) is essential for binding to HAP crystal surfaces. Removal of the DpSpSE moiety (SN-11, EKFLRRIGRFG) reduces the HAP binding affinity by a factor of 4.5 compared to SN-15. Mutation of both phosphoserines to simple serine reduces the HAP binding affinity by a factor of almost nine, while mutation to aspartic acid restores the binding affinity to 70% that of SN-15, indicating that the phosphoserine residues and acidic amino acid side chains are important for the binding of statherin to HAP.

Circular dichroism and solution NMR studies indicate that SN-15 is transiently helical in solution[24]. For this same moiety in HAP-bound statherin, measurement of a number of torsion angles and internuclear distances using solid state NMR indicate that the N-terminus is an α-helix[25–26]. Solid state NMR constraints and the Rosetta structure prediction algorithm have been used to obtain a model of the structure of HAP-bound statherin[27]. This model confirms the helicity of the N-terminus and attributes a helical structure to the C-terminus as well. Gray and coworkers[28] have developed a novel computational approach for modeling the interactions of statherin with HAP crystal surfaces. Using an all-atom Monte Carlo-minimization search algorithm to optimize rigid body and side chain conformations for binding to the 001 face of the HAP crystal, they predict side chain-surface interactions involving residues pS2, pS3, K6, R9, R10, R13, Y16, Q32, and P33. Solid state NMR[36] and calorimetric data[29] confirm the existence of some of these computationally-predicted protein-surface interactions including protein surface interactions involving several basic

amino acid side chains (e.g. K6, R9, R10, and R13) as well as several non-polar amino acids including L8 and F14[30,41].

In this paper, we augment our knowledge of the fundamental nature of protein-surface interactions by using $^{13}C\{^{31}P\}$ Rotational Echo DOuble Resonance (REDOR)[39] to directly detect distances between the carboxyl ^{13}C spins in glutamic acid side chains in statherin and ^{31}P spins located in the HAP crystal surface. Since dipolar recoupling of ^{13}C and ^{31}P via REDOR is effective over distances as great as 7 Å, the possibility exists that a given side chain carboxyl ^{13}C spin may couple to numerous ^{31}P spins in the HAP surface, which may complicate the analysis. Consistent with previous work involving similar interactions between the ε-^{15}N spin of the side chain of K6 and the HAP surface[40], fits between the side chain carboxyl ^{13}C spins in glutamic acid and several ^{31}P spins will be considered. This structural data is further supplemented by variable-temperature measurements of the rotating-frame spin-lattice relaxation time ($T_{1\rho}$), which are sensitive to the dynamics and solvent mobility near the ^{13}C label.

Materials and Methods

L-Glutamic-5-^{13}C acid, 99% enrichment (Figure 1A) was purchased from Isotec (Sigma-Aldrich). N-Fmoc-L-Glu-5-^{13}C-γ-tert-butyl ester (Figure 1B) was made using a four step protection and de-protection reaction described in the literature[31], with variations which resulted in considerably higher yield.

A: Synthesis of N-Fmoc-L-Glu-5-^{13}C Acid (2)

L-glutamic acid, 99% 5-^{13}C-labeled (0.970 g) was placed in a 100 mL round bottom flask with 15 mL of warm 10% aqueous sodium carbonate (Na_2CO_3) in which it was dissolved. Fmoc-OSu (9-fluorenyl methyl oxycarbonyl-N-hydroxysuccinimide, 2.70 g) was dissolved in 15 mL of dioxane and added to the amino acid solution. This mixture was stirred for 24 hours at room temperature. The solution was diluted with 100 mL of water and washed thrice with 50 mL of ethyl ether. The aqueous phase was acidified to pH 2 with 2 M HCl. The white solid was then extracted with 100 mL of ethyl acetate. Sodium chloride was added to the aqueous layer and again extracted with 50 mL of ethyl acetate. The combined ethyl acetate extractions were washed with brine, dried over magnesium sulfate, and concentrated. The N-Fmoc-glutamic acid, 5-^{13}C was confirmed with ^1H NMR (MeOH-d_4) and mass spectrometry. The product mass was 2.42 g (100% yield).

B: Synthesis of N-Fmoc-L-Glu-5-^{13}C γ-Benzyl Ester (3) and γ-Benzyl Ester (3')

N-Fmoc-L-Glu-5-^{13}C (2), (2.42 g, 6.5 mmol) and N,N'-Dicyclohexylcarbodiimide (1.34 g, 6.5 mmol) were dissolved in 5 mL tetrahydrofuran (THF) and mixed for 23 hours. The resulting mixture was filtered and the filtrate was evaporated leaving a crude anhydride. This material was dissolved in 5 mL of THF and the solution was treated with benzyl alcohol (1.40 mL) and potassium carbonate, K_2CO_3 (1.2 g, 8.96 mmol). After 5 hours, the reaction was filtered and the solid was washed with dichloromethane, and the resultant solution washed with 1N HCl and saturated brine, then dried. The crude residue on evaporation was chromatographed over silica gel (100 g), eluted first with 100% CH_2Cl_2 and then 3% MeOH / 97% CH_2Cl_2. The α-benzyl ester (2.0372 g, 75% yield) eluted first: ^1H NMR ($CDCl_3$) δ 1.7–2.6 (m, 4H), 4.0–4.6 (m 4H), 5.0–5.2 (s, 2H), 5.6–5.9 (d, 1H), 7.1–7.8 (m, 13H). The γ-benzyl ester (494.5 mg, 18% yield) eluted later, also characterized by ^1H NMR ($CDCl_3$).

C: Synthesis of N-Fmoc-L-Glu-5-^{13}C α-Benzyl, γ-tert-Butyl Ester (4)

N-Fmoc-L-Glu-5-^{13}C α-benzyl ester (3), (2.0372 g, 4.4 mmol), concentrated sulfuric acid (0.5 mL), and CH_2Cl_2 (20 mL) were added to a Parr bottle and cooled to −78°C in a dry ice-acetone bath. To this was added isobutylene (20 mL) condensed at −78°C. The resultant mixture was attached to a Parr apparatus and shaken for 23 hours at 25°C. The reaction was then vented, diluted with methylene chloride and extracted with 5% aqueous sodium bicarbonate ($NaHCO_3$). The organic layer was dried and evaporated. The crude residue was chromatographed over silica gel (200 g) and eluted with 20% ethyl acetate in *n*-hexane. The product (1.8794 g, 83% yield) was isolated as a colorless solid: ^{1}H NMR ($CDCl_3$) δ1.4 (s, 9H), 1.8–2.4 (m, 4H), 3.9–4.6 (m, 4H), 5.2 (s, 2H), 5.6–5.8 (d, 1H), 7.1–7.8 (m, 13H).

D: Synthesis of N-Fmoc-L-Glu-5-^{13}C γ-tert-Butyl Ester (5)

A hydrogenation reaction using N-Fmoc-L-Glu-5-^{13}C α-benzyl, γ-*tert*-butyl ester (4), (1.8794 g, 3.6 mmol), 10% Pd/C (200 mg) in methanol (30 mL), and tetrahydrofuran (30 mL) was performed at 50 psi for 5 hours. The reaction mixture was diluted with ethyl acetate and filtered over diatomaceous earth. The residue was washed with additional ethyl acetate, and the combined filtrates were evaporated. The crude product was chromatographed over silica gel (200 g) and eluted with 1:40:59 acetic acid: ethyl acetate: *n*-hexane, giving the product as a colorless solid (1.3839 g, 89% yield): ^{1}H NMR ($CDCl_3$) δ1.4 (s, 9H), 1.8–2.6 (m, 4H), 4.1–4.7 (m, 4H), 5.6–5.8 (d, 1H), 7.1–7.8 (m, 13H). The overall yield was 56%.

Statherin Synthesis

N-Fmoc-L-Glu-5-^{13}C γ-tert-butyl ester was used to synthesize three statherin samples: statherin[4-Glu[5-^{13}C]] (stE4), statherin[5-Glu[5-^{13}C]] (stE5), and statherin[26-Glu[5-^{13}C]] (stE26). Peptide synthesis was conducted on an automated synthesizer (Rainin PS3, Protein Technologies, Tucson, AZ) using standard Fmoc chemistry, with N-methyl-2-pyrrolidinone (NMP) as the solvent, 20% piperidine in NMP as the deprotecting reagent, and 0.4 M N-methylmorpholine in dimethyl formamide as the activating reagent. The solid phase support was Fmoc-Phe-TGA resin from Novabiochem (417 mg, 0.24 mmol/g substitution). Cleavage of the peptide from the solid support was achieved by stirring gently for 2 hours in a covered solution of 95% trifluoroacetic acid, 2.5% triisopropylsilane, and 2.5% water. The protein was precipitated from this solution in a cold (−20°C) solution of *tert*-butyl methyl ether.

Protein Purification

The protein was purified on a bioCAD SPRINT FPLC using a 10 mm × 100 mm, 7.9 mL, POROS HQ/M perfusion anion-exchange column. The mobile phase consisted of (A) 50 mM Tris-HCl at pH 8.5, (B) 0.5M NaCl and buffer A, (C) acetonitrile, with the latter held at 30% to maintain protein solubility. The crude peptide was dissolved in a mixture of 30% acetonitrile, 70% buffer A solution (10 mg peptide/mL), and 3 mL injection volumes into a 4 mL loop were utilized to load the column. A linear gradient from 0 to 70% B in 14.7 column volumes was used to elute the protein at a flow rate of 3 mL/min. UV absorption at a wavelength of 280 nm was used to detect the desired product, which eluted at 35% buffer B. The protein was then concentrated using a Centriplus 3 kDa MWCO centrifugal filter unit. Following purification, the sample was lyophilized, and then analyzed by mass spectrometry for composition and purity.

Statherin Binding to Hydroxyapatite (HAP, $Ca_{10}(H_2O)_2(PO_4)_6$)

Hydroxyapatite seed crystals were generously provided by W. Shaw and A. Campbell (Battelle Pacific Northwest National Laboratory, Richland, WA). X-ray powder diffraction

confirmed the formation of HAP and the absence of any undesired calcium phosphate phases. BET (Quantachrom) measurements showed a specific surface area of 57 m^2/g. Crystal morphology, as determined by electron microscopy (SEM and TEM), was as expected for synthetic hydroxyapatite with plate-like morphology terminating predominantly along the [001] face of the crystal.

Pure statherin was dissolved in PBS buffer (100 mM NaCl, 40 mM KCl, 4.3 mM Na_2HPO_4, 1.4 mM KH_2PO_4, pH 7.4) to maintain constant pH conditions at temperatures below the freezing point of water. Approximately 16 mg of protein were adsorbed by mixing 30 mg of the protein with 100 mg of hydroxyapatite in PBS for 4 hours. After centrifugation, the wet pellet containing the complex was washed three times with the phosphate buffer to remove all unbound protein. The mineral-protein complex was then flash-frozen with liquid nitrogen before insertion into a pre-cooled NMR probe to increase cross polarization efficiency while avoiding water crystallization or salt depletion. This approach is consistent with previous studies, which have indicated that the N-terminus of statherin exhibits no substantial changes in the secondary structure upon freezing[27]. For the remainder of this paper, we will refer to the samples as stE4hap, stE5hap, and stE26hap (after binding of the respective proteins to hydroxyapatite) while the samples of the free protein are referred to as stE4, stE5 and stE26 as defined in the materials and methods section.

NMR Experiments

Solid-state NMR experiments were performed on a home-built spectrometer attached to a 11.74 T superconducting magnet and operating at Larmor frequencies of 500.11 MHz for ^1H, 202.53 MHz for ^{31}P, and 125.76 MHz for ^{13}C. The ^{13}C NMR signal was enhanced using ramped cross polarization with a ^1H–^{13}C contact time of 1 ms. CP/MAS, REDOR, and $T_{1\rho}$ experiments were performed using a 4 mm HXY triple-resonance Varian T3 magic angle spinning probe. Unless otherwise stated, the sample temperature was held at −32° C. An XY8-phase cycling $^{13}C\{^{31}P\}$ REDOR sequence with alternating π-pulses in both the ^{13}C-observed and ^{31}P-dephasing channel was utilized (Figure 2). REDOR dephasing times were restricted to 12 ms. Pulse lengths were 3.25 μs for ^1H π/2 pulses, 7.0 μs for ^{13}C π pulses, and 8.3 μs for ^{31}P π pulses.

Simulations and Data Fitting

For ^{13}C experiments, the $T_{1\rho}$ value was extracted from a linear fit of the semi-log plot of the signal amplitude as a function of spin-lock time. For the REDOR data, numerical simulations of the experimental data were performed using the NMR simulation software SIMPSON[32] employing the direct algorithm without any relaxation. Powder averages were obtained using a minimal set of 232 {α, β} Euler angles specified by the Zaremba-Conroy-Wolfsberg scheme[33–34] and 10 γ angles. A chemical shift anisotropy (CSA) of 80 ppm and asymmetry parameter of 0.68 for the side chain carboxylate ^{13}C in glutamic acid, and 11.5 ppm and asymmetry of 0.9 for the phosphate ^{31}P in hydroxyapatite[35], were incorporated. Mutual orientations of the phosphorous CSA and dipolar interactions with respect to the carbon CSA tensor were neglected in all simulations. For stE4hap and stE26hap, the REDOR simulations were performed assuming dephasing by a single ^{31}P spin. For the stE5hap sample, where significant dephasing was observed experimentally, additional simulations were performed to account for the multiple phosphorous atoms encountered on the surface of HAP in the form of a pseudo-^{31}P-pair with a larger effective interaction as reported before[36]. See Figure 3. These spin triad simulations involved a pair of ^{31}P spins with an effective coupling of 600 Hz and one ^{13}C spin coupled to the two ^{31}P spins.

Results

^{13}C CPMAS Spectra of HAP-Bound Statherin

For the side chain carboxyl ^{13}C spins of glutamic acid at positions E4, E5, and E26 in free statherin, the isotropic chemical shift was observed in CPMAS experiments to be 179±1 ppm (data not shown) relative to TMS, which is within experimental error of the value obtained from the same spin species in polyglutamic acid[37]. Chemical shifts of ^{13}C spins in peptides change upon adsorption to mineral surfaces as a result of conformational changes of the peptide or as a result of protein-surface interactions.

Figures 4a,b show the ^{13}C carboxyl peak of stE4hap and stE5hap. A similar spectrum is shown in Figure 4c for glutamic acid (E). Principal values for the chemical shift anisotropy (CSA) tensors are given in Table 1.

While the carboxylate ^{13}C chemical shift in stE26 is invariant upon binding to HAP, remaining at about 179 ppm, the isotropic chemical shift of the carboxylate ^{13}C spins in stE4 and stE5 shift downfield to about 184 ppm upon binding. Assuming that a downfield shift of the carboxylate ^{13}C resonances in stE4hap and stE5hap result from deshielding due to a close approach to a positive charge center in the HAP surface, these chemical shift data indicate that the side chain carboxyl groups of E4 and E5 are closely associated with the HAP surface, while the carboxyl group of E26 is more removed.

$^{13}C\{^{31}P\}$ REDOR Studies of Interactions between Statherin Glutamic Acid Side Chains and HAP

The $^{13}C\{^{31}P\}$ REDOR pulse sequence[39] shown in Figure 2 was applied to all three HAP-bound samples in order to determine specific distances between individual protein spins and the surface. Results are shown in Figure 4. The REDOR data vary drastically as a function of position of the 5-^{13}C-glutamic acid in the primary sequence of statherin. The behavior observed for stE4hap and stE26hap are essentially identical: for both, the intensity of the side chain carboxylate ^{13}C signal slowly diminishes to about 90% of its S_0 intensity as a result of REDOR irradiation for recoupling times in excess of 12 ms. In contrast, for stE5, the intensity of the side chain carboxyl ^{13}C signal rapidly diminishes to about 10% of its S_0 intensity after only 5.8 ms. The REDOR data observed in Figure 4 indicate that the side chain carboxyl ^{13}C spins in stE4hap and stE26hap are far more removed from ^{31}P spins than is the case for the corresponding ^{13}C spin in stE5hap.

The data in Figure 5 have at least three explanations. We can conclude from it that in contrast to stE4hap and stE26hap, the side chain carboxyl ^{13}C spin in stE5hap is: 1) dephased by one or both of the ^{31}P spins located in the phosphoserine side chains; 2) dephased by at least one ^{31}P spin located in the HAP surface; 3) dephased by a combination of phosphoserine and HAP ^{31}P spins.

Neither stE4 nor stE5 dephased under $^{13}C\{^{31}P\}$ REDOR irradiation, indicating that when not adsorbed onto HAP, the distances between the ^{31}P spins in the side chains of pS2 and pS3 are too great (>>7 Å) to result in observable dephasing. These observations, however, do not indicate with certainty that the phosphoserine side chains do not contribute to the dephasing of the carboxylate ^{13}C in E5, as the phosphoserine and glutamate side chains could change conformation upon adsorption to HAP, a possibility that invalidates the REDOR study of stE5 as a control.

The possible involvement of ^{31}P spins from phosphoserine residues of statherin was also encountered in the analysis of $^{15}N\{^{31}P\}$ REDOR data acquired from the ε-^{15}N in the K6 side chain of statherin adsorbed onto HAP crystals[40]. In that case, the likely proximity of a

pS side chain to the K6 side chain was obtained from a statistical analysis of 31 low energy structures predicted using *de novo* energy minimization techniques from the Rosetta program[41–43] The possibility of a $^{15}N\{^{31}P\}$ REDOR effect between the ε-^{15}N of K6 and the ^{31}P in the side chains of either pS2 or pS3 was excluded because only 1 of 31 predicted structures show a distance even as close as 4.5 Å between the K6 ^{15}N and the pS3 oxygen in an unphosphorylated SN-15 sample. All the other structures showed distances greater than 5 Å. Insofar as none of the computationally predicted distances between the ε-^{15}N and phosphoserine ^{31}P spins resulted in a dipolar coupling large enough to simulate the $^{15}N\{^{31}P\}$ REDOR data, it was concluded that HAP ^{31}P spins were responsible for most of the dephasing observed in the $^{15}N\{^{31}P\}$ REDOR experiment.

A similar but more rigorous analysis was performed to determine the possibility of a $^{13}C\{^{31}P\}$ REDOR effect between the ^{13}C carboxylate spin of E5 and the side chains of pS2 and/or pS3. The minimum energy structure obtained for statherin on 001 HAP reported recently by Gray and coworkers using the RosettaSurface program[27] yields predicted distances between glutamic acid carboxylates and phosphoserine phosphate groups, which along with their predicted dipolar coupling constants are summarized in Table 2.

A 6.5 Å ^{13}C–^{31}P internuclear distance results in a 45 Hz dipolar coupling constant. This indicates that the ^{31}P spins in phosphoserines 2 and 3 cannot account for the amount of $^{13}C\{^{31}P\}$ REDOR dephasing observed for the carboxylate ^{13}C spin in stE5hap.

Assuming ^{31}P spins from HAP dominate the $^{13}C\{^{31}P\}$ REDOR observed for the stE5hap sample, the size of the ^{31}P dephasing system must be determined in order to simulate a REDOR curve. In $^{15}N\{^{31}P\}$ REDOR studies of diammonium hydrogen phosphate (DHP) and of HAP-bound SN-15[36] with the ε amino group in the side chain of K6 enriched with ^{15}N, it was found that accurate nearest neighbor ^{15}N–^{31}P heteronuclear couplings could be determined even when the ^{31}P dephasing system was truncated to two ^{31}P spins. Simulations of known distributions of ^{15}N and ^{31}P spins in DHP, for example, show that accurate heteronuclear dipolar couplings to the two nearest neighbor ^{31}P spins can be extracted from a truncated ^{31}P dephasing system assuming a ^{31}P–^{31}P dipolar coupling of 600 Hz.

Following this strategy, simulations of the REDOR data using both an isolated ^{13}C–^{31}P spin pair model, and a ^{13}C–^{31}P–^{31}P triad (see Figure 3), are shown in Figure 6a–c. χ^2 plots of the family of fits for the three models shown are shown below as Figure 6d–f. Figure 6a shows results for the isolated ^{13}C–^{31}P pair model for ^{13}C–^{31}P dipolar coupling values ranging from 220 to 275 Hz. Close agreement with the data is obtained for a ^{13}C–^{31}P dipolar coupling of 245 Hz, corresponding to a ^{13}C–^{31}P internuclear distance of about 3.7 Å. The χ^2 plot in Figure 6d shows a minimum at about 3.75 ± 0.10 Å for the isolated ^{13}C–^{31}P spin pair model. Figures 6b and 6c show simulation scenarios for the 3 spin CPP clusters assuming ^{31}P–^{31}P dipolar couplings of 0 Hz and 600 Hz. For a ^{31}P–^{31}P dipolar coupling of 0 Hz, the best fit to the REDOR data is achieved assuming two equivalent ^{13}C–^{31}P dipolar couplings of 170 Hz, corresponding to a ^{13}C–^{31}P distance of about 4.2 ± 0.1 Å each, as the χ^2 plot in Figure 6e shows. A more realistic model using a truncated ^{31}P system, represented as two ^{31}P spins with a 600 Hz ^{31}P–^{31}P coupling, also achieves a best fit for two equivalent ^{13}C–^{31}P couplings, but the χ^2 plot in Figure 6f shows the best fit ^{13}C–^{31}P distance for the 600 Hz ^{31}P–^{31}P dipolar coupling case is shifted to a slightly longer distance of 4.25 ± 0.09 Å.

^{13}C Side Chain Carboxyl Spin Dynamics

Although the large extent and indeterminate nature of the ^{31}P dephasing network does not allow unique determination of the number and magnitude of ^{13}C–^{31}P dipolar couplings

between the side chain carboxyl ^{13}C spins in statherin and the ^{31}P spins of the HAP surface, comparison of the $^{13}C\{^{31}P\}$ REDOR data for stE4hap, stE5hap, and stE26hap show that only the side chain of E5 likely lies within 4.0–4.5 Å of the HAP surface. It is therefore interesting to directly compare the trend in $^{13}C\{^{31}P\}$ REDOR data with the trend in glutamic acid side chain dynamics, as probed by ^{13}C rotating frame ($T_{1\rho}$) relaxation measurements. $T_{1\rho}$ measurements, when applied during MAS, can site-specifically elucidate polymer motions on the time scale of the r.f. field amplitude applied to the carboxyl ^{13}C spins. In the present study, the amplitude is 71 kHz.

Figure 7 shows the dependence of side chain carboxyl ^{13}C $T_{1\rho}$ on temperature and position of the labeled glutamic acid side chain in the primary sequence of statherin. For temperatures between 220K and 280K, $T_{1\rho}$ varies with primary sequence position as:

stE26hap < stE4hap < stE5hap.

At ambient temperature, the $T_{1\rho}$s of stE4hap and stE26hap are both about 12 ms, while $T_{1\rho}\approx 28$ ms for stE5hap. For temperatures above 273K, $T_{1\rho}$ for all three sites increases as the temperature increases, placing all three ^{13}C spins in a dynamic regime where $\omega_1\tau < 1$, where ω_1 is the amplitude of the r.f. field and τ is a generalized correlation time of the ^{13}C–^{1}H vector motion. At temperatures lower than 273K, $T_{1\rho}$ increases as the temperature decreases, indicating that $\omega_1 \tau > 1$.

Because at ambient temperature all three glutamic acid sites are in the fast motion regime, i.e. $1/\tau >> \omega_1$, the rotating frame relaxation rate will depend most strongly on dynamic amplitudes as opposed to the rates of motion. Therefore, in the fast regime, we expect differences in rotating frame relaxation rates to be reflected by differences in the principal values of magnetic interaction tensors that have been pre-averaged by fast side chain motions. Inspection of the CSA data for the side chain carboxyl groups of stE4hap and stE5hap versus polycrystalline glutamic acid elucidate the origins of the $T_{1\rho}$ trend for these amino acid side chains. First, the principal values of both stE4hap and stE5hap are identical to within experimental error. The chemical shift tensors of carboxylate ^{13}C spins are some of the best studied and most thoroughly reported in the literature[38]. For example, ^{13}C NMR studies of single crystals of oxalic acid dehydrate (HOX) and diammonium oxalate monohydrate (DAOX)[44] report not only the principal values of the CSA tensors of those compounds, but also the orientation of the principal axis systems relative to molecule-fixed frames. In DAOX, δ_{11} is within 3 degrees of the C–C bond axis and nearly bisects the O–C–O angle. Although the carboxylate CSA tensor orientation can vary from compound to compound as a result of local structural variations, the general trend in many carboxylate compounds is that δ_{22} is oriented close to the O–C–O bond, while δ_{33} is to varying degrees oriented most closely to the normal vector to the O–C–O plane.

If the observed $T_{1\rho}$ difference between stE4hap and stE5hap were attributable to differential side chain motion occurring at rates fast enough to effect rotating frame relaxation, the rate of such motions would exceed the CSAs for both sites, and we would expect to observe predictable differences in the motionally pre-averaged CSA principal values for stE4hap and stE5hap. For example, one of the best studied instances of large amplitude side chain motions in solid proteins is the dynamics of the isopropyl groups in the side chains of leucine amino acids in collagen fibers[45]. The exchange of the leucine side chain isopropyl groups between two rotational bond conformers produces a change in the orientation of the C_γ–$C_{\delta 1}$ and C_γ–$C_{\delta 2}$ bond axes by about 109°. If the side chains of stE4hap and stE5hap displayed differential mobility, we would expect profound differences in the pre-averaged principal values. However, their CSA tensors are virtually identical. This argues that the motions of these side chains are similar and thus the modulations of dipolar couplings between the carboxylate ^{13}C spins and nearest neighbor protons on the C_γ carbons are

similar in the side chains of stE4hap and stE5hap and are unlikely to account for the large $T_{1\rho}$ difference between the stE4hap and stE5hap sites.

Although the data in Table 1 indicate that the motions of the glutamic acid side chains of statherin do not differ significantly, there is every reason to believe that the proximity of water to these side chains is quite different. Using an isothermal titration calorimetry study, Goobes et al.[46], found that the adsorption of the statherin N-terminal fragment SN-15 is nearly thermal-neutral and that the binding of SN-15 to the HAP surface is entropically driven. A small enthalpy of adsorption and a large positive entropy of adsorption occur when protein side chains expel water and ions from the HAP surface. In the present case this means that while stE4hap and stE26hap, both of which are oriented away from the HAP surface and into the solvent, are surrounded by water; but stE5HAP, which is oriented close to the HAP surface, is very likely more remote from water. We conclude that at least for stE4hap and stE5hap, for which we have accurate CSA values and thus some quantitative probe of local side chain motional differences, it is unlikely that the observed $T_{1\rho}$ difference arises from differential side chain mobility alone if at all.

Discussion

Solid state NMR has been used in several prior cases to study the spin dynamics of glutamic acid-rich proteins adsorbed onto HAP crystals. For example, Fernandez and coworkers[37] used both CP/MAS and ^{13}C $T_{1\rho}$ measurements to study the adsorption of polyglutamic acid onto HAP and silica particles. In a series of papers by Duer and coworkers, $^{13}C\{^{31}P\}$ REDOR was used to elucidate the role of glutamic acid side chains in the binding of proteins to HAP particles[47] as well as the interactions between the protein and mineral components of bone[35]. While these prior studies succeeded in identifying and characterizing properties unique to glutamic acid residues in proximity to a HAP surfaces, these studies also generally applied solid state NMR techniques to ^{13}C spins at natural abundance and therefore were not site selective. This present study differs from prior work on acidic proteins adsorbed onto HAP in that here the glutamic acid sites are individually interrogated using $^{13}C\{^{31}P\}$ REDOR to detect specific surface contacts, and ^{13}C $T_{1\rho}$ relaxation measurements are used to comparatively study the dynamics of individual glutamic acid side chains. How do the results of the present study differ from these other studies and to what degree does it extend our knowledge of how proteins interact and recognize biomineral surfaces in general and HAP in particular?

There are two scenarios that would cause variation of $T_{1\rho}$ between different carboxyl side chains in statherin. Both scenarios originate with the degree of proximity of the given carboxylate side chain to the HAP surface. First, differences in local motions of glutamic acid side chains would result in differential modulation of dipolar couplings between the carboxylate ^{13}C spins and protons located on the glutamic acid side chain. Therefore, $T_{1\rho}$ differences between carboxylate ^{13}C spins of E4, E5, and E26 may reflect differences in local motions of the glutamic acid side chains. Second, differences in the structure and modulation of the proton bath near to each side chain carboxyl ^{13}C spin may also modulate $T_{1\rho}$ relaxation. This situation would arise if the distribution and or dynamics of water molecules near to the unprotonated carboxylate ^{13}C spins varied between E5 and the other glutamic acid side chains. Prior studies of the dynamics and hydration of statherin on HAP surfaces indicate that both scenarios are plausible and likely occur with the glutamic acid side chains.

Prior solid state REDOR and $T_{1\rho}$ studies of protonated ^{13}C spins in the phenyl side chains of F7 and F14 in SN-15 adsorbed onto HAP[48] indicated differences in the rate of side chain dynamics between a phenyl side chain adjacent to the HAP surface versus a phenyl side

chain oriented away from the surface In that study, $^{13}C\{^{31}P\}$ REDOR was also used to determine proximity to the HAP surface. The REDOR study showed that the F14 phenyl ring is about 4 Å from the nearest ^{31}P spin in the HAP surface, while the F7 phenyl showed no measureable dephasing during $^{13}C\{^{31}P\}$ REDOR irradiation and thus was determined to be greater than 6.5–7.0 Å from the HAP surface. Because the ^{13}C spins in the side chains of F7 and F14 that were observed under cross polarization conditions are covalently protonated, the interpretation of $T_{1\rho}$ data is less ambiguous than in the case of the carboxyl ^{13}C spins of this study, because modulation of the dipolar coupling between the phenyl ring ^{13}C spins and their directly bonded protons would dominate $T_{1\rho}$ relaxation. A study of $T_{1\rho}$ measured as a function of temperature showed that the F7 ^{13}C spins lie on the fast side of the $T_{1\rho}$ minimum ($\omega_1\tau < 1$) while F14 was on the slow side ($\omega_1\tau < 1$), indicating that proximity to the HAP surface perturbs the rates of side chain dynamics in F14 versus F7.

In the case of E4 and E5, which are both situated on a segment of statherin that is largely immobilized on HAP, the CSAs are identical to within experimental error and unlike F7 and F14, the motions of both side chains are in the fast limit. Both observations indicate that the local motions of E4 and E5 are similar in amplitude amplitude and rate. The possible role of solvent motions in $T_{1\rho}$ relaxation of the glutamic acid side chains is elucidated by a isothermal titration calorimetric study[46] by Goobes et al. This ITC study showed that while HAP adsorption of statherin is accompanied by a very small enthalpy of adsorption at low protein coverages and is virtually thermal-neutral at higher coverages, there also occurs a large positive entropy of adsorption. The positive entropy change does not reflect changes in the structural state of statherin upon adsorption because the protein is unstructured in solution and only folds into a permanent structure upon adsorption onto HAP. Rather, the positive entropy of adsorption reflects the expulsion of water and ions from the hydrophilic surface upon adsorption of protein. This means that E5, which is oriented close to the surface, is likely more remote from water than are E4 and E26, which are oriented away from the surface and thus are solvent-exposed. Regardless of which mechanism is responsible for the difference between the $T_{1\rho}$ relaxation of E5 versus E4/E26, the origin undoubtedly lies with the difference between the environment of the protein side chain near to the HAP surface versus the environment remote from the surface.

It is also interesting to compare our results to those of Duer and coworkers who also have performed $^{13}C\{^{31}P\}$REDOR on proteins adsorbed onto HAP particles[47] and on bone[35]. One of the model peptides studied by Duer was poly-aspartic acid (PD) adsorbed onto HAP particles. The strong dephasing of the carbonyl and side chain carboxyl ^{13}C signals of PD during $^{13}C\{^{31}P\}$ REDOR irradiation indicated that PD displaces enough water from the HAP surface to enable it to bind closely itself to the surface. In another $^{13}C\{^{31}P\}$ REDOR study of bone, they observed strong dephasing of the carboxyl ^{13}C signal arising from the protein component of bone during $^{13}C\{^{31}P\}$ REDOR irradiation. From these REDOR data the average distance between the carboxyl ^{13}C spins of the protein component and the ^{31}P spins of the mineral component was estimated to be 4.5–5.0 Å.

Our $^{13}C\{^{31}P\}$ REDOR data for stE5hap bear that out to the extent that we also detect a carboxyl ^{13}C–^{31}P distance of about 4.2 Å, which is close to that found in bone. However, the aggregate results obtained from DRAWS studies of SN-15 and $^{15}N\{^{31}P\}$ and $^{13}C\{^{31}P\}$ of interactions between basic and nonpolar side chains with HAP, in addition to calorimetric studies of the effect of Arg to Ala mutations on the binding of SN-15 to HAP, indicate an intricate mode of interaction between statherin and HAP. This may involve some nonpolar amino acid side chains as well as the phosphoserines, the basic side chains, and some acidic side chains in the N-terminus of statherin. When these ssNMR and calorimetric data are combined with the results of computational studies of statherin on HAP[27], a model emerges,

shown in Figure 8, which explains how the secondary structure of the N-terminus enables exposure of selected side chains in the N-terminus to the HAP surface. According to the distorted α–helical secondary structure that we have proposed, the side chains of E5, K6, and F14 are within 4.0–4.2 Å of the HAP surface, while the side chains of E4 and F7 are more than 6–7 Å from the surface. In addition, isothermal titration calorimetric studies indicate a reduced binding affinity between statherin mutants in which R9, R10, and R13 are replaced with alanines. Such mutants do not show marked changes in secondary structure, so the implication is that these arginine side chains are also involved in interactions with the HAP surface.

Conclusion

We have used REDOR NMR to show that the side chain of E5 are in close contact with the HAP surface and have estimated this distance to be 4.25 Å. In contrast, the side chains of E4 and E26 show weak REDOR dephasing, indicating that they are further removed from the surface. We have also used ^{13}C $T_{1\rho}$ measurements to demonstrate a slower rotating-frame relaxation rate for E5 compared to E4 and E26. This slower relaxation is attributed to restriction in side chain dynamics and/or displacement of water near the HAP surface. Based on this and prior data, we have proposed a model of the binding of statherin to HAP in which the N terminus of statherin adopts a distorted α-helical structure. Further studies involving other side chains in statherin and the role of water at the protein-HAP interface are underway.

Acknowledgments

We thank Dr. Allison Campbell and Dr. Wendy Shaw for the hydroxyapatite sample. This research was supported by National Institutes of Health grants RO1 DE12554-06 and RO1-GM074511-03.

References

1. Schoen FJ, Levy RJ. Ann. Thorac. Surg. 2005; 79:1072–1080. [PubMed: 15734452]
2. Coe FL, Parks JH, Asplin JR. N. Engl. J. Med. 1992; 327:1141–1152. [PubMed: 1528210]
3. McCarty DJ. DM-Dis. Mon. 1994; 40:259–299.
4. Giachelli CM. J. Am. Soc. Nephrol. 2004; 15:2959–2564. [PubMed: 15579497]
5. Margolis HC, Beniash E, Fowler CE. J. Dent. Res. 2006; 85:775–793. [PubMed: 16931858]
6. He G, Gajjeraman S, Schultz D, Cookson D, Qin CL, Butler WT, Hao JJ, George A. Biochemistry. 2005; 44:16140–16148. [PubMed: 16331974]
7. Matsumoto T, Okazaki M, Inoue M, Sasaki J, Hamada Y, Takahashi J. Dent. Mater. J. 2006; 25:360–364. [PubMed: 16916241]
8. Addadi L, Joester D, Nudelman F, Weiner S. Chem.-Eur. J. 2006; 12:981–987.
9. Cha JN, Shimizu K, Zhou Y, Christiansen SC, Chmelka BF, Stucky GD, Morse DE. Proc. Natl. Acad. Sci. U. S. A. 1999; 96:361–365. [PubMed: 9892638]
10. Beniash E, Simmer JP, Margolis HC. J. Struct. Biol. 2005; 149:182–190. [PubMed: 15681234]
11. Alford AI, Hankenson KD. Bone. 2006; 38:749–757. [PubMed: 16412713]
12. Giachelli CM, Steitz S. Matrix Biol. 2000; 19:615–622. [PubMed: 11102750]
13. Palmer LC, Newcomb CJ, Kaltz SR, Spoerke ED, Stupp SI. Chem. Rev. 2008; 108:4754–4783. [PubMed: 19006400]
14. Koutsopoulos S, Dalas E. J. Crystal Growth. 2000; 217:410–415.
15. Sugino A, Miyazaki T, Ohtsuki C. J. Mater. Sci: Mater. Med. 2008; 19:2269–2274. [PubMed: 18058198]
16. Olszta MJ, Douglas EP, Gower LB. Calcif. Tissue Int. 2003; 72:583–591. [PubMed: 12616327]
17. Olszta MJ, Odom DJ, Douglas EP, Gower LB. Connect. Tissue Res. 2003; 44:326–334. [PubMed: 12952217]

18. Bradt JH, Mertig M, Teresiak A, Pompe W. Chem. Mater. 1999; 10:2694–2701.
19. Quin C, D'Souzar R, Feng JQ. J. Dent. Res. 2007; 86:1134–1141. [PubMed: 18037646]
20. Gibson CW, Yuan ZA, Hall B, Longenecker G, Chen E, Thyagarajan T, Sreenath T, Wright JT, Decker S, Piddington R, Harrison G, Kulkarni AB. J. Biol. Chem. 2001; 276:31871–31875. [PubMed: 11406633]
21. Shaw WJ, Ferris K, Tarasevich B, Larson JL. Biophys. J. 94; 8:3247–3257.
22. Wikiel K, Burke EM, Perich JW, Reynolds EC, Nancollas GH. Arch. Oral Biol. 1994; 39:715–721. [PubMed: 7980121]
23. Raj PA, Johnsson M, Levine MJ, Nancollas GH. J. Biol. Chem. 1992; 267:5968–5976. [PubMed: 1313424]
24. Douglas WH, Reeh ES, Ramasubbu N, Raj PA, Bhandary KK, Levine MJ. Biochem. Biophys. Res. Commun. 1991; 180:91–97. [PubMed: 1718282]
25. Shaw WJ, Long JR, Dindot JL, Campbell AA, Stayton PS, Drobny GP. J. Amer. Chem. Soc. 2000; 122:1709–1716.
26. Long JR, Shaw WJ, Stayton PS, Drobny GP. Biochemistry. 2001; 40:15451–15455. [PubMed: 11747419]
27. Goobes G, Goobes R, Schueler-Furman O, Baker D, Stayton PS, Drobny GP. Proc. Natl. Acad. Sci. U. S. A. 2006; 103:16083–16088. [PubMed: 17060618]
28. Makrodimitris K, Masica DL, Kim ET, Gray JJ. J. Am. Chem. Soc. 2007; 129:13713–13722. [PubMed: 17929924]
29. Goobes R, Goobes G, Shaw WJ, Drobny GP, Campbell CT, Stayton PS. Biochemistry. 2007; 46:4725–4733. [PubMed: 17391007]
30. Goobes G, Goobes R, Gibson JM, Long JR, Paranji R, Popham JM, Raghunathan V, Shaw WJ, Campbell CT, Stayton PS, Drobny GP. Mag. Res. Chem. 2007; 45:S32–S47.
31. Kelly RC, Gebhard I, Wicnienski N. J. Org. Chem. 1986; 51:4590–4594.
32. Bak M, Rasmussen JT, Nielsen NC. J. Magn. Reson. 2000; 147:296–330. [PubMed: 11097821]
33. Conroy H. J. Chem. Phys. 1967; 47:5307.
34. Cheng VB, Suzukawa HH, Wolfsberg M. J. Chem. Phys. 1973; 59:3992–3999.
35. Best SM, Duer MJ, Reid DG, Wise ER, Zou S. Magn. Reson. Chem. 2008; 46:323–329. [PubMed: 18306171]
36. Raghunathan V, Gibson JM, Goobes G, Popham JM, Louie EA, Stayton PS, Drobny GP. J. Phys. Chem. B. 2006; 110:9324–9332. [PubMed: 16671751]
37. Fernandez VL, Reimer JA, Denn MM. J. Am. Chem. Soc. 1992; 114:9634–9642.
38. Duncan, TM. Compilation of Chemical Shift Anisotropies. Chicago: The Farragut Press; 1990. p. 3
39. Gullion T, Schaefer J. J. Magn. Reson. 1989; 81:196–200.
40. Gibson JM, Raghunathan V, Popham JM, Stayton PS, Drobny GP. J. Amer. Chem. Soc. 2005; 127:9350–9351. [PubMed: 15984845]
41. Rohl CA, Strauss CEM, Misura KMS, Baker D. Methods Enzym. 2004; 383:66–93.
42. Schueler-Furman O, Wang C, Bradley P, Misura K, Baker D. Science. 2005; 310:638–642. [PubMed: 16254179]
43. Bradley P, Misura KMS, Baker D. Science. 2005; 309:1868–1871. [PubMed: 16166519]
44. Griffin RG, Pines A, Pausak S, Waugh JS. J. Chem. Phys. 1975; 63:1267–1271.
45. Batchelder LS, Sullivan CE, Jelinski LW, Torchia DA. Proc. Natl. Acad. Sci. USA. 1982; 79:386–389. [PubMed: 6952191]
46. Goobes R, Goobes G, Campbell CT, Stayton PS. Biochemistry. 2006; 45:5576–5586. [PubMed: 16634639]
47. Jaeger C, Groom NS, Bowe EA, Horner A, Davies ME, Murray RC, Duer MJ. Chem. Mater. 2005; 17:3059–3061.
48. Gibson JM, Popham JM, Raghunathan V, Stayton PS, Drobny GP. J. Am. Chem. Soc. 2006; 128:5364–5370. [PubMed: 16620107]

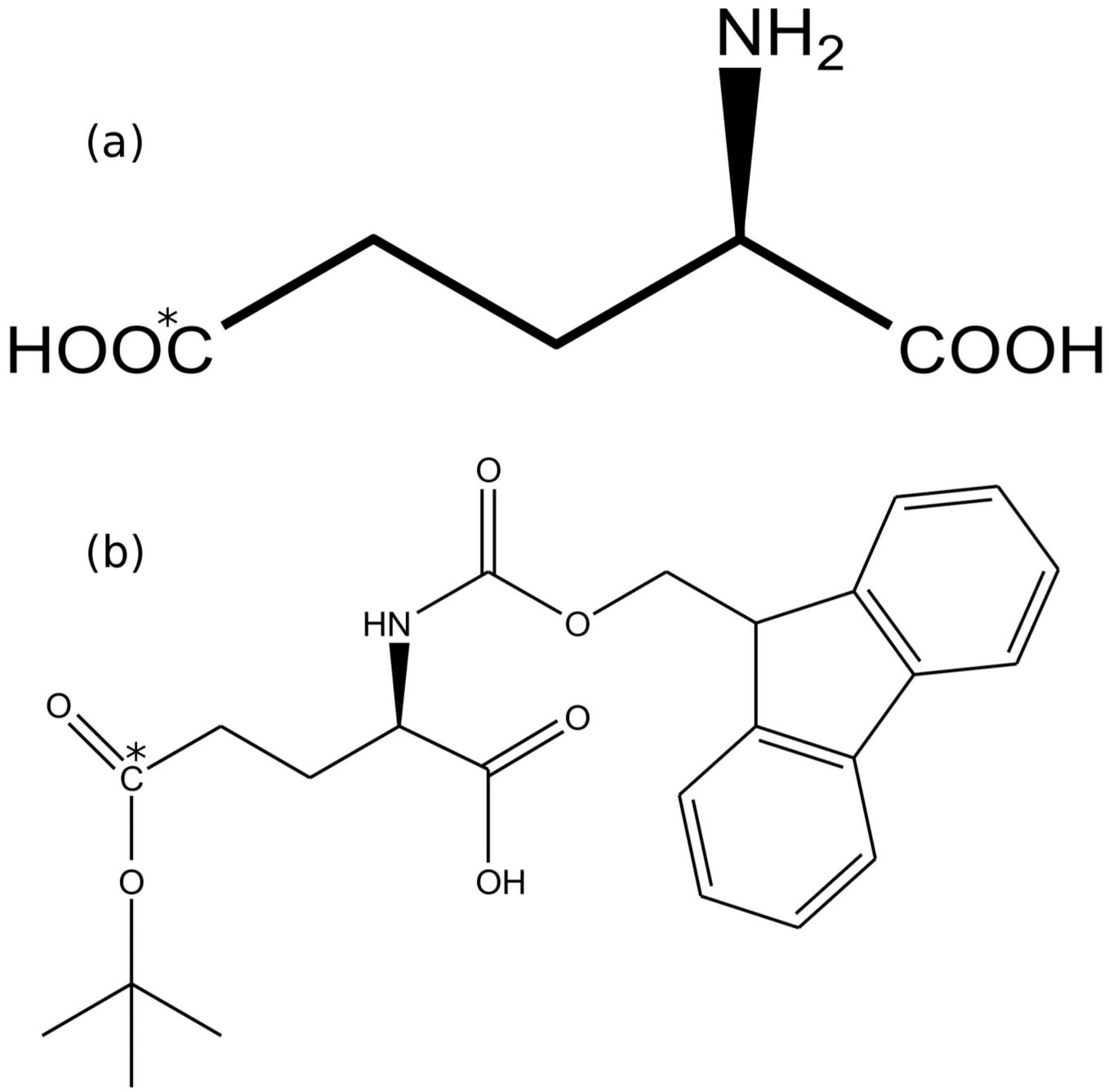

Figure 1.
Structure of (a) glutamic acid, 5-^{13}C, (b) Fmoc-glutamic acid (5-^{13}C) t-butyl ester. ^{13}C labeled site indicated with asterisk.

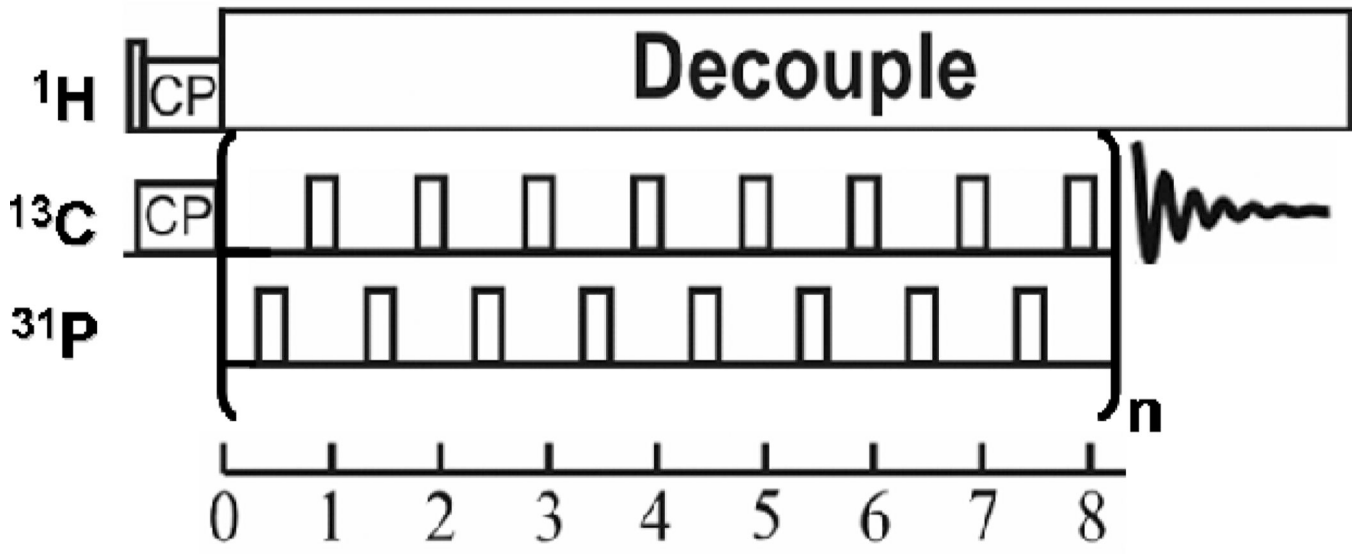

Figure 2.
XY8 phase cycling $^{13}C\{^{31}P\}$ REDOR pulse sequence with alternating π pulses.

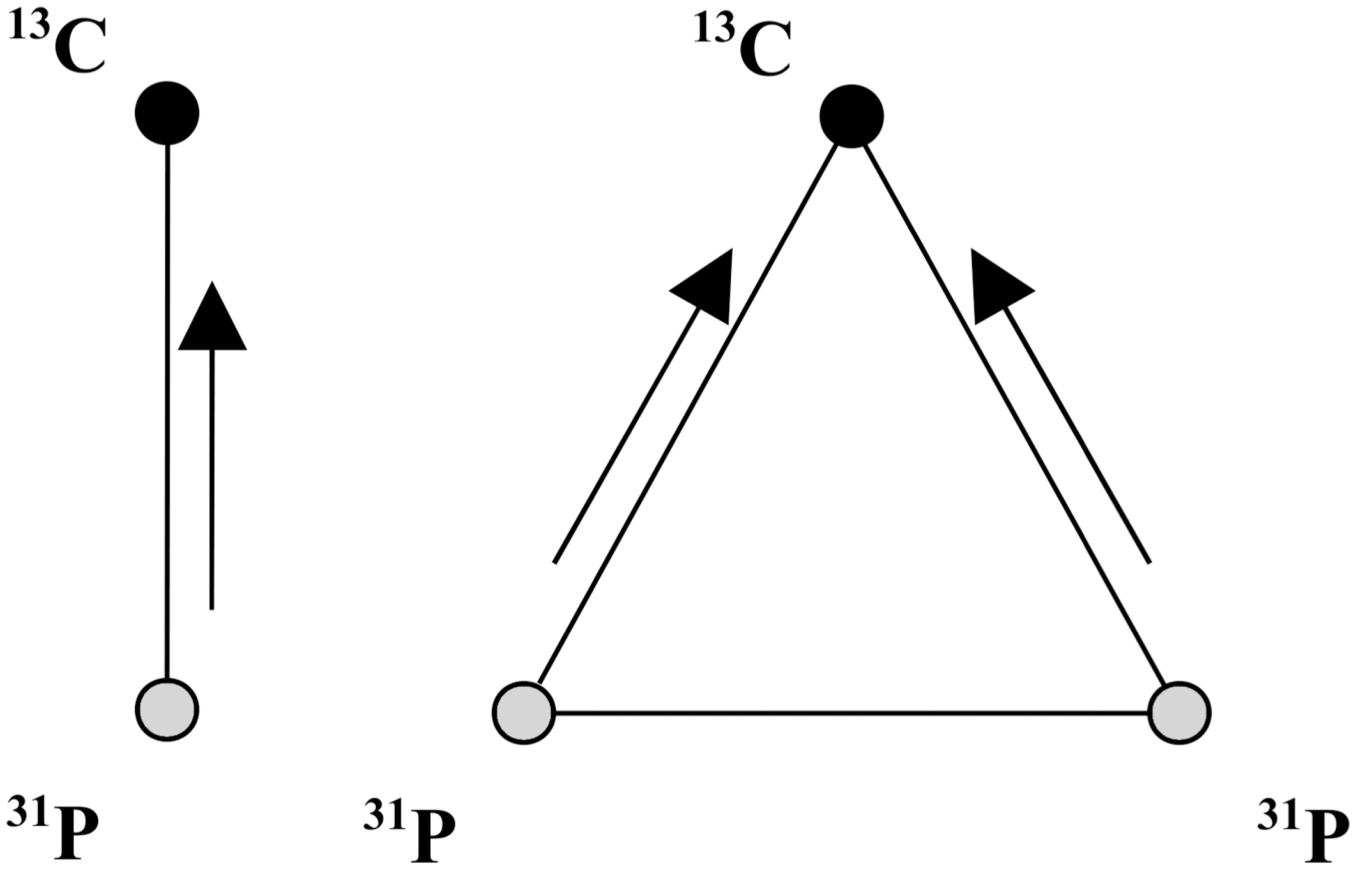

Figure 3.
^{31}P spin topologies used in simulation of ^{13}C{^{31}P} REDOR data. Arrows in the figure indicate the dipolar couplings that were varied in simulations. Homonuclear coupling of pseudo-^{31}P-pair was fixed at 600 Hz based on previous studies[36].

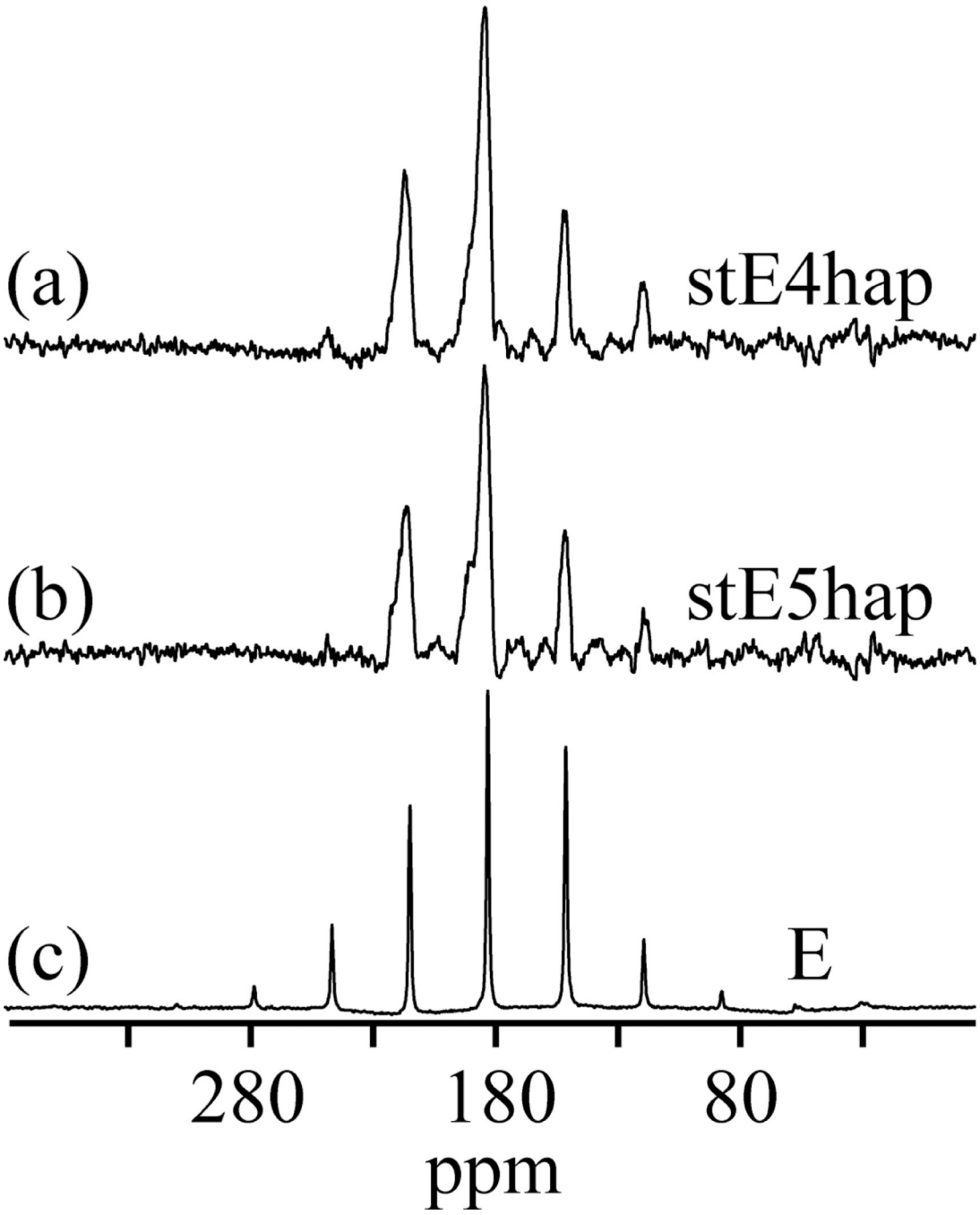

Figure 4.
CPMAS spectra of stE4hap, stE5hap, and polycrystalline glutamic acid (E) acquired at room temperature and a spinning rate of 4 kHz.

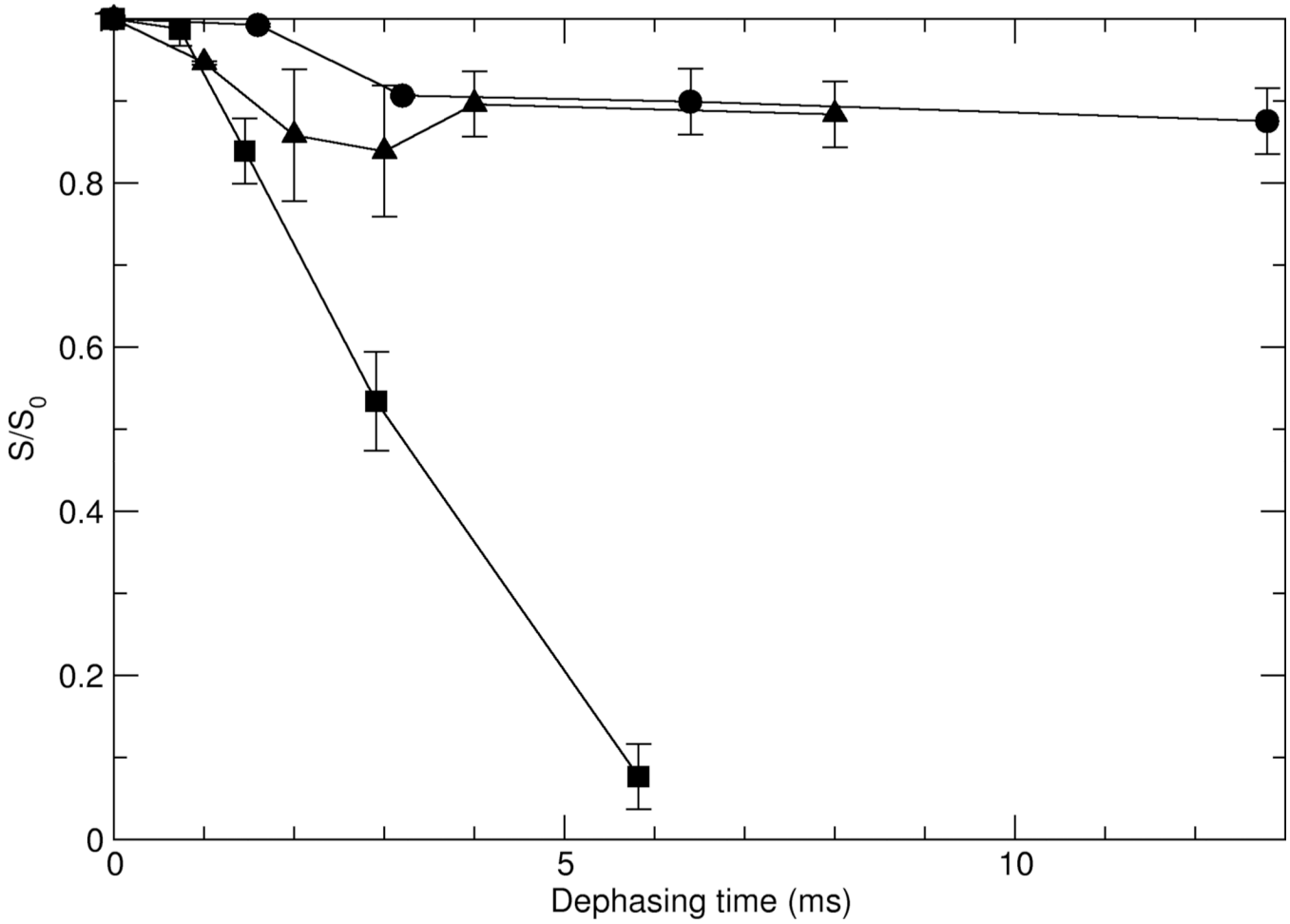

Figure 5.
REDOR decay plots for the three statherin samples bound to HAP. Circles indicate stE4hap, squares indicate stE5hap, and triangles indicate stE26hap.

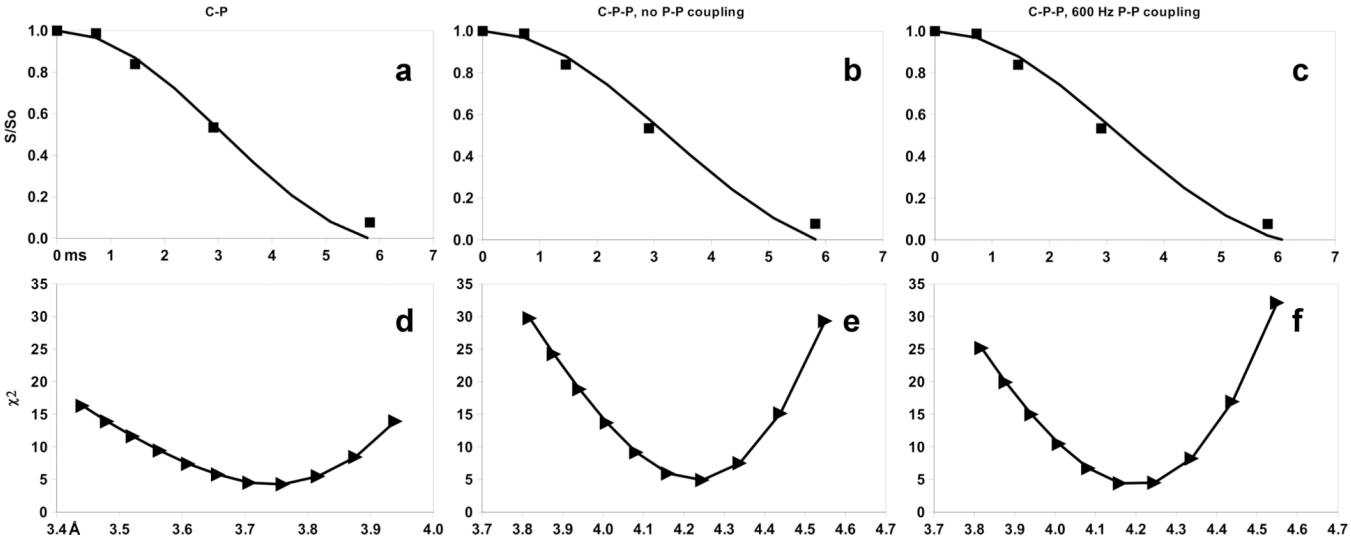

Figure 6.

Simulated $^{13}C\{^{31}P\}$ REDOR curves for three possible spin systems: (a) 2-spin $^{13}C–^{31}P$ coupling, (b) 3-spin coupling of one ^{13}C to two ^{31}P nuclei without any $^{31}P–^{31}P$ coupling, (c) 3-spin $^{13}C–^{31}P–^{31}P$ coupling with fixed 600 Hz $^{31}P–^{31}P$ coupling. Experimental stE5hap data (square symbols) are depicted in (a) – (c) as well. (d) through (f) are the corresponding χ^2 values calculated and plotted based on simulations carried at each value of the C–P internuclear distance (Å) shown by the triangle symbols.

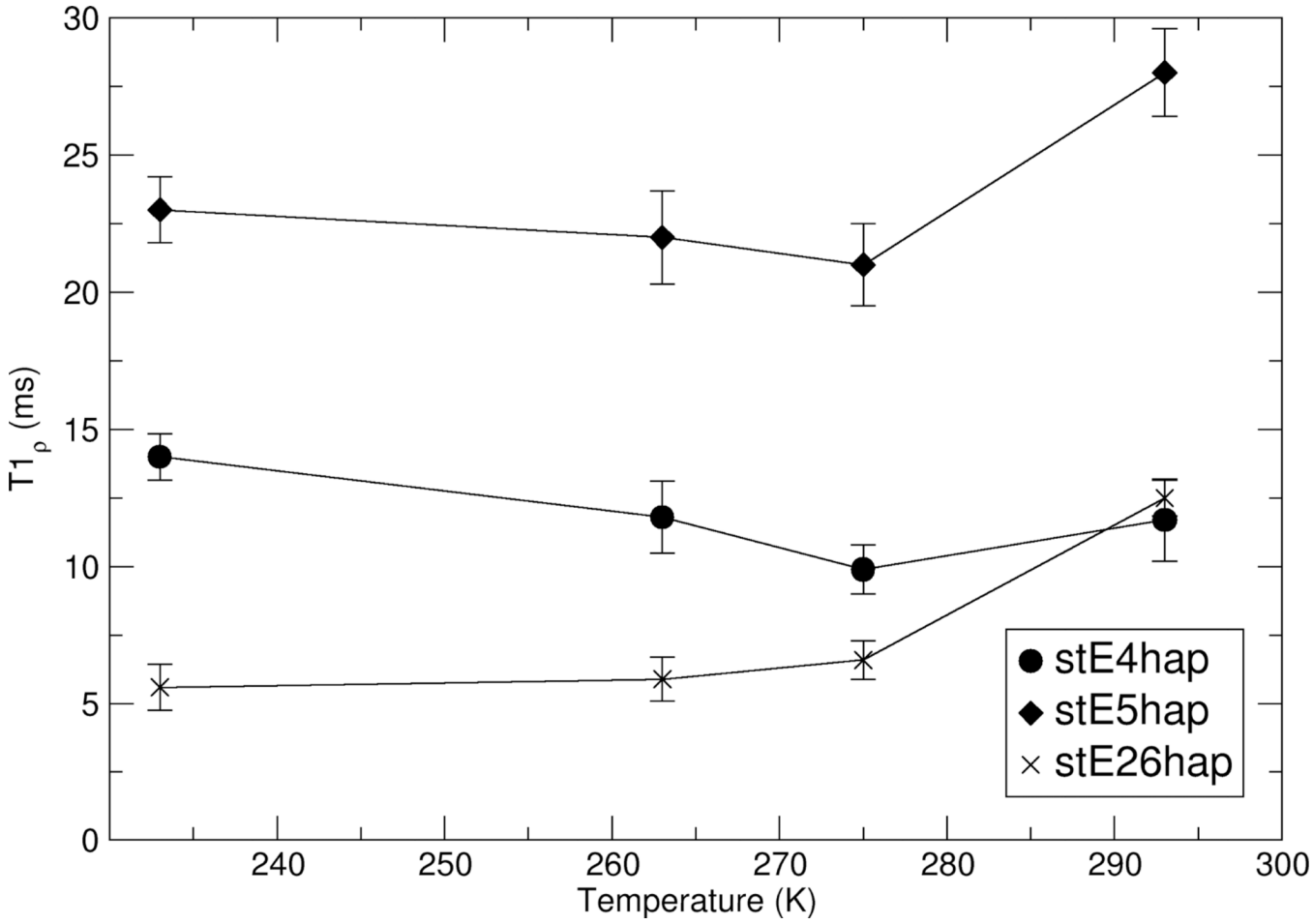

Figure 7.
HAP-bound statherin $T_{1\rho}$ values for E4, E5, and E26 as functions of sample temperature.

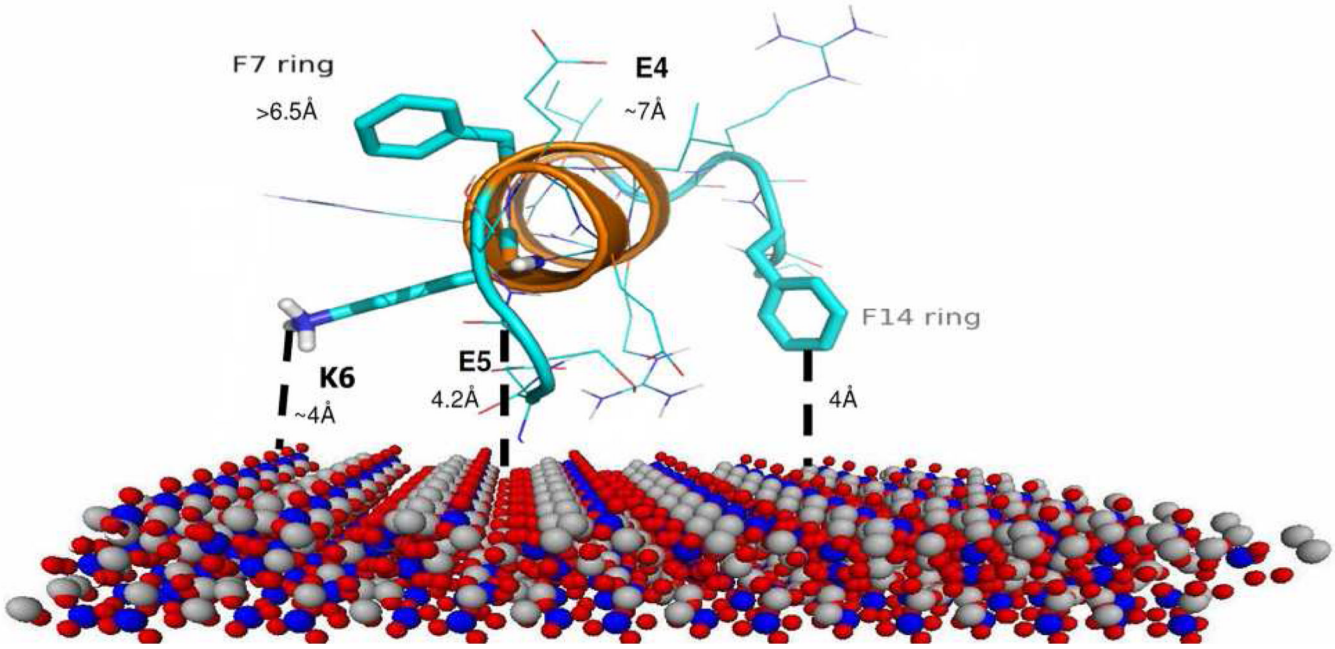

Figure 8.
Model of N-terminal region of statherin on HAP surface, combining new and previously established distance constraints.

Table 1

Principal values for the ^{13}C CSA tensors of stE4hap, stE5hap, and glutamic acid (E) relative to TMS. The anisotropy and asymmetry calculations assumed the convention observed in Duncan[38].

Sample	δ_{11} (ppm)	δ_{22} (ppm)	δ_{33} (ppm)	δ_{iso} (ppm)	CSA (ppm)	η
stE4hap	251 ± 6	184 ± 6	118 ± 6	184 ± 1	100 ± 10	1.0 ± 0.1
stE5hap	253 ± 6	183 ± 6	116 ± 6	184 ± 1	104 ± 10	1.0 ± 0.1
E	261 ± 3	172 ± 3	114 ± 3	182.0 ± 0.2	118 ± 5	0.7 ± 0.1

Table 2

Simulated distances between glutamic acid carboxylate sites and phosphoserine phosphate sites in statherin based on lowest-energy Rosetta structure, with dipolar coupling for those distances.

Residue Pair	Distance	Coupling
E4–pS2	12.0 Å	7.1 Hz
E4–pS3	8.5 Å	20 Hz
E5–pS2	12.0 Å	7.1 Hz
E5–pS3	6.5 Å	45 Hz